J. Fluid Mech. (1970), *vol.* 41, *part* 4, *pp.* 769–792
Printed in Great Britain

An analytic solution for two- and three-dimensional wings in ground effect

By SHEILA E. WIDNALL
AND TIMOTHY M. BARROWS
Massachusetts Institute of Technology

(Received 11 July 1969)

The method of matched asymptotic expansions is applied to the problem of a wing of finite span in very close proximity to the ground. The general lifting surface problem is shown to be a direct problem, represented by a source-sink distribution on the upper surface of the wing and wake, with concentrated sources around the leading and side edges plus a separate confined channel flow region under the wing and wake. The two-dimensional flat plate airfoil is examined in detail and results for upper and lower surface pressure distribution and lift coefficient are compared with a numerical solution. A simple analytic solution is obtained for a flat wing with a straight trailing edge which has minimum induced drag. To lowest order, this optimally loaded wing has an elliptical planform and a lift distribution which is linear along the chord, resulting in a parabolic spanwise lift distribution. An expression for the lift coefficient at small clearance and angle of attack, valid for moderate aspect ratio, is derived. The analytic results show reasonable agreement when compared with numerical results from lifting surface theory.

1. Introduction

The possibility of using aerodynamic forces to support a high-speed ground-transportation vehicle gives rise to an interesting class of problems in which a lifting surface translates in close proximity to a solid boundary. Figure 1 shows two ground-transportation vehicle concepts which illustrate operation in open and enclosed guideways. The finite aspect ratio wing close to the ground (figure 2) can be considered the simplest three-dimensional problem in this class.

The term 'ram wing' has been applied to the earliest vehicles which were designed to utilize the ground effect principle. Among the first of these was a craft built by Kaario (1935) which was large enough to carry one man, and flew successfully over the ice on a lake in Finland.

Several investigators have attempted solutions to the ground effect problem using a variety of methods. An interesting survey of some of the earliest investigations has been provided by Pistolesi (1937). The two-dimensional problem is amenable to solution by complex variables although the solutions obtained tend to be unwieldy. The farthest advance along this line is the work by Tomotika, Hasimoto & Urano (1951). The linearized problem is also amenable to solution

by a distribution of singularities with suitable images placed below the ground plane. One of the best examples of this approach for the two-dimensional case has been given by Bagley (1960). (This work is a good source of further references.) In three dimensions this method results in a problem suitable for lifting surface theory (cf. Ashley & Landahl 1965) with solutions generally requiring a high-speed computer.

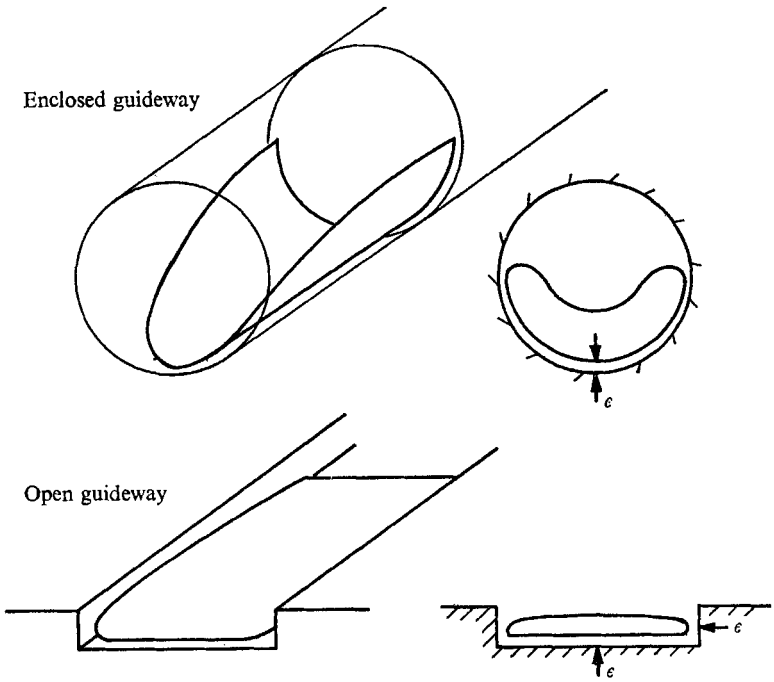

FIGURE 1. High speed ground transportation vehicles in close proximity to solid boundaries.

All of these approaches are quite reasonable for wings which are not too close to the ground, such as might be encountered with an airplane during takeoff or landing. However, when a lifting surface is designed to take advantage of ground effect the greatest interest lies in very close proximity, and in this case it is possible to introduce certain simplifications. Strand, Royce & Fujita (1962) showed that for the case of a two-dimensional airfoil in close proximity the flow in the narrow region between the wing and the ground, which was termed 'channel flow', becomes one-dimensional. This pleasing and simple result has one drawback: no method is presented to determine the total amount of mass flow under the wing without solving the entire flow problem.

In the present paper a small parameter ϵ is defined as the ratio of the ground clearance to the chord, and the linearized ground effect problem is solved using the method of matched asymptotic expansions. It is shown that for a wing at angle of attack α, the vertical flow perturbations are of $O(\alpha)$, while in the confined region under the wing this vertical velocity of $O(\alpha)$ induces a horizontal

velocity of $O(\alpha/\epsilon)$. In the case of the two-dimensional airfoil (figure 3) the one-dimensional nature of the lowest order solution for the channel flow (preserving the notation of Strand) becomes immediately apparent. However, there are obviously regions near the leading and trailing edges where the flow reverts to a two-dimensional state. Hence, for these 'inner regions' (inner in the sense of

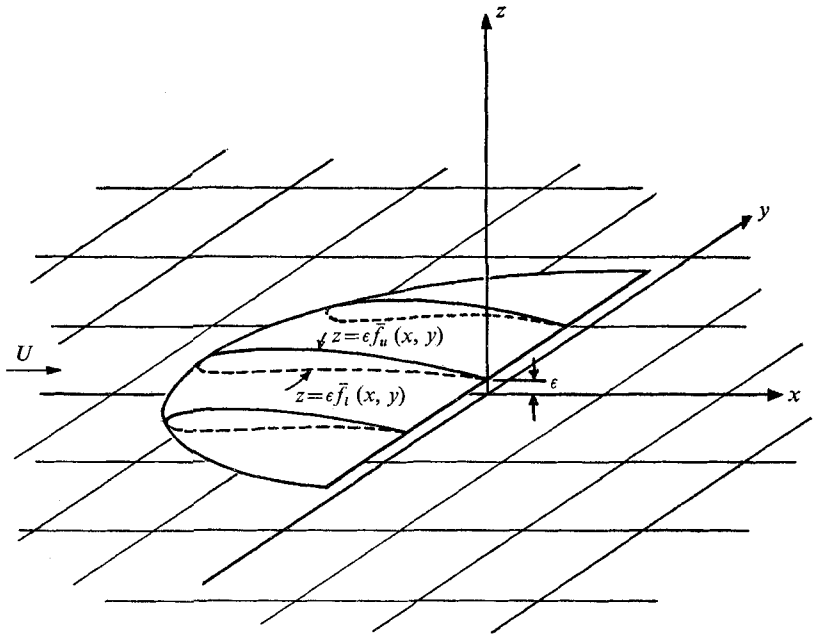

FIGURE 2. Lifting surface in close proximity to the ground.
$\bar{f}_l(x,y) = 1+(\alpha/\epsilon)\bar{g}_l(x,y)$, $\bar{f}_u(x,y) = 1+(\alpha/\epsilon)\bar{g}_u(x,y)$.

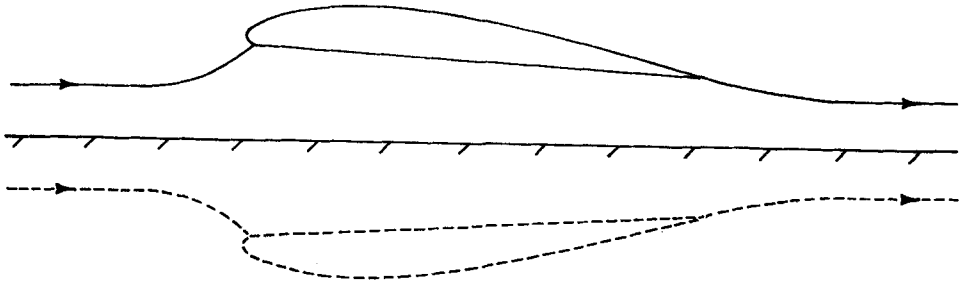

FIGURE 3. Flow past a two-dimensional airfoil in ground effect.

asymptotic expansions) special expansions are required, which are called edge flow solutions. These solutions are matched to the channel flow solution below the wing and to the outer flow above the wing.

Considering the outer region and its image, it is clear that the flow must be symmetrical about the line $z = 0$, z being the vertical, so that in the case of $\epsilon \ll 1$ the outer flow can be represented by a distribution of sources and sinks along the x axis. It also turns out that a concentrated source is required at the

leading edge, representing the upward deflexion of the stagnation streamline. An important feature is that this becomes a direct problem, involving a known source distribution, rather than an indirect problem involving an unknown vortex distribution, so that even for a general airfoil the difficulties of inverting an integral equation are avoided. As shown in § 4, for a flat plate airfoil the method yields a relatively simple analytic solution which gives the pressure distribution over the upper and lower surfaces.

These ideas are extended to three dimensions. In this case the flow under the wing and trailing vortex wake, which we shall persist in calling the channel flow, is two dimensional in the x, y plane. The edge flow solutions must be applied along the side edges of the wing and wake as well as along the leading and trailing edges. In the outer region, the flow can be represented by a known distribution of sources and sinks on the wing and wake surface plus a distribution of concentrated sources around the leading and side edges, whose strength is determined by matching.

The method can be extended to cover more complex configurations operating in enclosed or open guideways to obtain analytic predictions of the aerodynamic characteristics of these vehicles. The ground effect theory which follows from showing that the channel flow is two dimensional in the x, y plane forms an interesting complement to Jones's slender body theory and Prandtl's lifting line theory, in which the flows are basically two dimensional in the y, z and x, z planes, respectively. Both of these classical perturbation theories, incidentally, can be derived using matched asymptotic expansions (Van Dyke 1964 and Ashley & Landahl 1965).

2. Problem formulation—the general problem

The finite wing in close proximity to the ground in an incompressible flow is sketched in figure 2. There are two possible versions of this problem for the region beneath the wing, the linear and non-linear problems. In the linear problem, the displacements of the under surface must be small in comparison to the clearance to chord ratio. This version is compatible with linearized lifting surface theory in which the lowest order solution everywhere is a free stream and the upwash boundary conditions are satisfied on the mean plane of the wing, at a height ϵ above the ground. In the non-linear problem, the displacements of the under surface are of the order of the clearance. The lowest order solution for the flow beneath the wing is not a uniform stream and the flow tangency boundary condition must be satisfied on the actual lower surface. This latter problem is more difficult and is currently under investigation. The linear problem will be examined in this paper and the results compared with numerical lifting surface theory.

The wing upper and lower surfaces are described by

$$\left.\begin{aligned} S_l(x,y,z) &= z-\epsilon\bar{f}_l(x,y) = 0 \quad \text{on lower surface,} \\ S_u(x,y,z) &= z-\epsilon\bar{f}_u(x,y) = 0 \quad \text{on upper surface,} \end{aligned}\right\} \tag{2.1}$$

where $\bar{f}_{u,l}(x,y) = 1+(\alpha/\epsilon)\,\bar{g}_{u,l}(x,y)$, $\bar{g}_{u,l}(x,y)$ is an $O(1)$ function describing the distribution of camber, angle of attack and thickness on the airfoil. x, y, z are

co-ordinates normalized by the midchord of the wing, ϵ is the ratio of height to chord and the subscripts l and u denote lower and upper surface respectively.

The boundary condition of flow tangency is

$$\nabla\Phi \,.\, \nabla S_{u,l}(x,y,z) = 0 \quad \text{on} \quad S_{u,l}(x,y,z) = 0, \tag{2.2}$$

On the ground we require $$\partial\Phi/\partial z = 0, \tag{2.3}$$

where Φ is the velocity potential normalized by U, satisfying Laplace's equation

$$\nabla^2\Phi = 0. \tag{2.4}$$

To determine a perturbation solution valid for the region beneath the wing where z is $O(\epsilon)$, the z co-ordinate is stretched. That is

$$\bar{z} = z/\epsilon \quad \text{and} \quad \frac{\partial\Phi^c}{\partial\bar{z}} = \epsilon\frac{\partial\Phi}{\partial z}, \tag{2.5}$$

where Φ^c is the potential in the channel under the wing. The governing equation for Φ^c becomes

$$\frac{1}{\epsilon^2}\frac{\partial^2\Phi^c}{\partial\bar{z}^2} + \nabla_{2D}^2\,\Phi^c = 0, \tag{2.6}$$

where ∇_{2D} is the two-dimensional operator $\mathbf{i}\,\partial/\partial x + \mathbf{j}\,\partial/\partial y$. The boundary condition of flow tangency on the lower surface for Φ^c is

$$\frac{\partial\Phi^c}{\partial\bar{z}} = \epsilon\alpha\nabla_{2D}\,\bar{g}_l(x,y)\,.\,\nabla_{2D}\,\Phi^c \quad \text{at} \quad \bar{z} = 1 + \frac{\alpha}{\epsilon}\,\bar{g}_l(x,y). \tag{2.7}$$

There are two small parameters in this problem, α, the angle of attack, and ϵ, the clearance. If $\alpha \sim O(\epsilon)$, the boundary conditions must be satisfied on the actual under surface of the wing, if $\alpha \sim o(\epsilon)$, a Taylor series expansion of the boundary conditions about $\bar{z} = 1$ is permitted (Van Dyke 1964) and an ordinary linear lifting surface problem is obtained. To compare with numerical lifting surface theory, only terms linear in α would be appropriate.

An asymptotic expansion of the form

$$\begin{aligned}\Phi^c(x,y,\bar{z}) = x + (\alpha/\epsilon)\,\phi_1^c + \alpha f_1(\epsilon)\,\phi_2^c + \alpha\phi_3^c + \ldots \\ + \alpha\epsilon\phi_4^c + \alpha\epsilon^2 f_1(\epsilon)\,\phi_5^c + \alpha\epsilon^2\phi_6^c \ldots,\end{aligned} \tag{2.8}$$

or $$\Phi^c(x,y,\bar{z}) = x + \alpha\phi^c$$

will be assumed. In the actual development of the solution, the form of the series was determined at each stage in the process as outlined in Van Dyke (1964). From the matching with the edge solutions, $f_1(\epsilon)$ turns out to be $\ln(1/\epsilon)$. ϕ_1^c, ϕ_2^c and ϕ_3^c will determine the lift coefficient on the wing to $O(\alpha)$. Equation (2.6) relates each ϕ_n^c to a ϕ_m^c two powers higher in ϵ. Thus, as will be seen, to solve for ϕ_1, ϕ_2 and ϕ_3 it is necessary to obtain the form of ϕ_4, ϕ_5 and ϕ_6. Intermediate solutions lying between ϕ_3 and ϕ_4 will not affect this procedure. The first non-zero boundary condition from (2.7) is applied to ϕ_4^c.

Before examining further the flow beneath the wing we consider the outer flow, which is a straightforward thin wing flow in both the linear and non-linear

problems

$$\Phi^o = x + \alpha\phi^o + \ldots. \tag{2.9}$$

The boundary condition to be satisfied on the plane $z = 0$ are

$$\left.\begin{aligned} \frac{\partial\phi^o}{\partial z} &= -\frac{\partial\bar{g}_u}{\partial x} \quad \text{at} \quad z = 0 \quad \text{on} \quad S, \\ \frac{\partial\phi^o}{\partial z} &= -\alpha_i(x,y) \quad \text{at} \quad z = 0 \quad \text{on} \quad W, \\ \frac{\partial\phi^o}{\partial z} &= 0 \quad \text{elsewhere}, \end{aligned}\right\} \tag{2.10}$$

where S and W are the projections of the wing and wake surfaces on $z = 0$. $\alpha_i(x, y)$ is the induced downwash in the wake due to the trailing vortex system. The singularities used to satisfy these boundary conditions are sources and sinks rather than the elementary horseshoe vortices which appear for the lifting problem for a wing far from the ground. In addition to the distribution of sources and sinks there are eigensolutions, concentrated sources (or sinks) of unknown strength located around the leading edge of the wing and side edges of the wake. These are absent at the trailing edge of the wing to lowest order because of the Kutta condition. Their purpose is to replace the fluid which has been removed by the excess of distributed sinks on the wing and wake surfaces. All of the properties of the outer flow potential ϕ^o can be found by solving lower order inner problems. The important feature of the outer flow is its very weak, $O(\alpha)$, influence on the inner flow. Because of this the Kutta condition requires $\partial\phi_1^c/\partial x = 0$ at the trailing edge.

We now state the sequence of problems and boundary conditions associated with the flow beneath the wing and wake. Substituting the assumed form (2.8) of Φ^c into the governing equation (2.6) and equating like functions of ϵ gives a very simple set of partial differential equations for the ϕ_n^c's.

$$\partial^2\phi_n^c/\partial\bar{z}^2 = 0 \quad (0 \leqslant n \leqslant 3). \tag{2.11}$$

Since $\partial\phi^c/\partial\bar{z} = 0$ at $\bar{z} = 0$, the solutions to these equations are simply functions of x and y.

$$\phi_n^c = \phi_n^c(x,y) \quad (0 \leqslant n \leqslant 3). \tag{2.12}$$

For the next order solutions the governing equations are

$$\left.\begin{aligned} \partial^2\phi_4^c/\partial\bar{z}^2 &= -\nabla_{2D}^2\phi_1^c(x,y), \\ \partial^2\phi_5^c/\partial\bar{z}^2 &= -\nabla_{2D}^2\phi_2^c(x,y), \\ \partial^2\phi_6^c/\partial\bar{z}^2 &= -\nabla_{2D}^2\phi_3^c(x,y). \end{aligned}\right\} \tag{2.13}$$

Since $\partial\phi^c/\partial\bar{z} = 0$ at $\bar{z} = 0$, the solutions for ϕ_4^c, ϕ_5^c and ϕ_6^c are

$$\left.\begin{aligned} \phi_4^c &= -\tfrac{1}{2}\bar{z}^2\nabla_{2D}^2\phi_1^c(x,y) + \tilde{\phi}_4^c(x,y), \\ \phi_5^c &= -\tfrac{1}{2}\bar{z}^2\nabla_{2D}^2\phi_2^c(x,y) + \tilde{\phi}_5^c(x,y), \\ \phi_6^c &= -\tfrac{1}{2}\bar{z}^2\nabla_{2D}^2\phi_3^c(x,y) + \tilde{\phi}_6^c(x,y), \end{aligned}\right\} \tag{2.14}$$

where $\tilde{\phi}_n^c$ is, at this stage, some arbitrary function of x and y. We now apply the flow tangency conditions on the under surface of the wing. This will give a set of equations for the unknown functions ϕ_n^c $(n = 1, 2, 3)$. The boundary conditions

for these equations are obtained by matching with the outer flow around the edges of the wing and wake surfaces through an edge flow region. The flow tangency condition of (2.7) expanded as a Taylor series about $\bar{z} = 1$ becomes

$$\frac{\partial \Phi^c}{\partial \bar{z}}(x, y, 1) + \frac{\partial^2 \Phi^c}{\partial \bar{z}^2}(x, y, 1)\frac{\alpha}{\epsilon}\bar{g}_l(x, y) + \ldots$$
$$= \epsilon\alpha \nabla_{2D}\bar{g}_l(x, y) \cdot \nabla_{2D}\Phi^c(x, y, 1) + \ldots. \tag{2.15}$$

Using the assumed form for Φ^c and equating like functions of α and ϵ, the boundary conditions for ϕ_4^c become

$$\frac{\partial \phi_4^c}{\partial \bar{z}} = \frac{\partial \bar{g}_l}{\partial x} \quad \text{at} \quad \bar{z} = 1. \tag{2.16}$$

The boundary conditions for ϕ_5^c and ϕ_6^c are

$$\frac{\partial \phi_5^c}{\partial \bar{z}} = 0, \quad \frac{\partial \phi_6^c}{\partial \bar{z}} = 0 \quad \text{at} \quad \bar{z} = 1. \tag{2.17}$$

Using the solutions for ϕ_4^c, ϕ_5^c and ϕ_6^c of (2.14) in (2.16) we obtain essentially a set of partial differential equations for ϕ_1^c, ϕ_2^c and ϕ_3^c. For $\phi_1^c(x, y)$

$$\nabla_{2D}^2 \phi_1^c(x, y) = -(\partial \bar{g}_l/\partial x)(x, y). \tag{2.18}$$

Physically this equation can be interpreted as conservation of mass in the two-dimensional region beneath the wing with known distributed mass addition provided by the flow tangency boundary condition on the lower surface.

From the boundary conditions of (2.17) and the relation between ϕ_2^c and ϕ_5^c and ϕ_6^c and ϕ_3^c given by (2.14), ϕ_2^c and ϕ_3^c satisfy Laplace's equation

$$\nabla_{2D}^2 \phi_2^c(x, y) = 0, \quad \nabla_{2D}^2 \phi_3^c(x, y) = 0, \tag{2.19}$$

i.e. two-dimensional potential flow under the wing.

Across the trailing vortex wake, the discontinuity in potential, $\Delta\phi$, must be a function of y only. Since the outer flow perturbations are $O(\alpha)$, the perturbation potentials ϕ_1^c and ϕ_2^c, which are valid beneath the wake for distances behind the trailing edge greater than ϵ, are likewise functions of y only. However, ϕ_3^c is in general a function of x and y since the outer flow potential ϕ_1^o which contributes to $\Delta\phi(y)$ is a function of x near the wing. In the wake, (2.18) and (2.19) become

$$\left.\begin{aligned} d^2\phi_1^c/dy^2 &= \alpha_i(y) \\ d^2\phi_2^c/dy^2 &= \alpha_{2i}(y), \\ \nabla^2\phi_3^c &= \alpha_{3i}(x, y). \end{aligned}\right\} \tag{2.20}$$

These equations are interpreted as equations for the induced downwash α_i for a known vortex strength in the wake; α_{2i} and α_{3i} are higher order contributions.

To summarize, the relations, equations and flow tangency boundary conditions have yielded (2.18) and (2.19) for the lowest order solutions ϕ_1^c to ϕ_3^c. The equation governing ϕ_1^c is that of conservation of mass in the two-dimensional channel beneath the wing with a known mass addition. The other functions are governed by Laplace's equation for two-dimensional potential flow under the wing with no mass addition. From these solutions we can find the expression for the pressure

on the underside of the wing. We can also solve for the structure of the wake and the strength of the edge sources in the outer flow. Inspection of the outer flow and edge flow solutions indicates that the boundary condition to be satisfied on the edges of the two-dimensional channel which represents the underside of the wing and wake are

$$\left.\begin{aligned} \phi_1^e &= 0 \quad \text{at the leading and side edges,} \\ \partial\phi_1^e/\partial x &= 0 \quad \text{at the trailing edge.} \end{aligned}\right\} \tag{2.21}$$

The boundary conditions on ϕ_2^e and ϕ_3^e on the edges bounding the confined region under the wing are more complex and must be obtained from matching with the outer flow potential ϕ^o through the edge flow solutions.

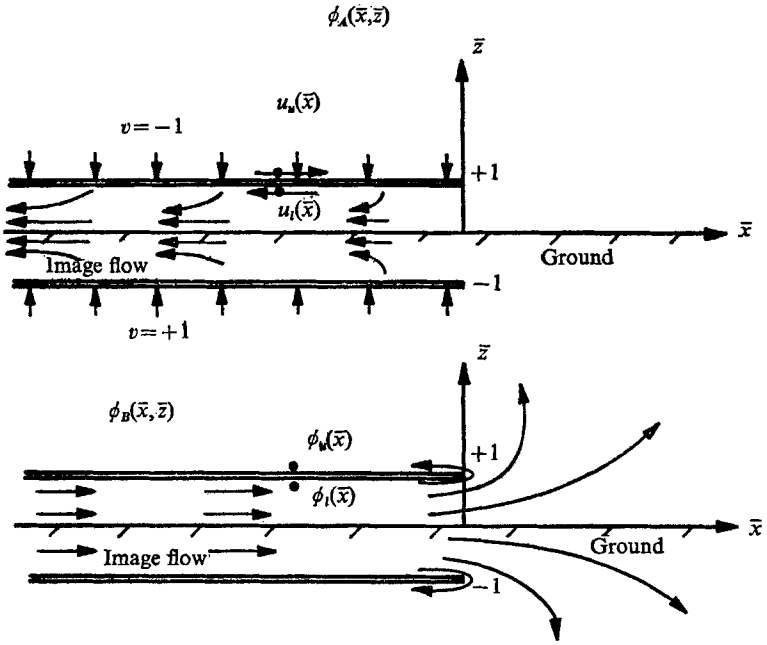

FIGURE 4. Two-dimensional incompressible edge flow problems valid near the end of a flat wing in ground effect. (*a*) $\bar{x}_{\text{on the plate}} = u + (1/\pi)[1 - e^{u\pi}]$; (*b*) $\bar{x}_{\text{on the plate}} = \phi + (1/\pi)[1 - e^{\phi\pi}]$.

3. Edge flow solutions

As previously discussed, the flow near the edges of the wing assumes a form different from either the outer flow or the channel flow and these regions require special inner expansions. For a two-dimensional flow in the x, z plane, these are obtained using the magnified complex variable

$$\overline{Y} = \bar{x} + i\bar{z},$$

where $\bar{x} = x/\epsilon$ and $\bar{z} = z/\epsilon$. That is, we now magnify x as well as z in order to focus on the properties of the inner region near the edge. For a general three-dimensional wing, $\bar{x}$ would be replaced by a local co-ordinate $\bar{n}$ normal to the edge.

The edge flows may be written in the following form (see figure 4)

$$\phi^i = \epsilon\phi_A + a_1\phi_B + a_2\bar{x} + a_3, \tag{3.1}$$

where ϕ^i = potential in the inner region,
ϕ_A = solution which satisfies the downwash condition $\partial\phi/\partial\bar{z} = -1$ on the wing,
ϕ_B = eigensolution with homogeneous boundary conditions—no velocity normal to the wing or the ground,
$\bar{x}$ = a local free stream,
a_n = constants to be determined by matching.

The solutions ϕ_A and ϕ_B may both be obtained using the following transformation

$$\left.\begin{aligned} \overline{Y} &= \eta + (1/\pi)[1 + e^{\eta\pi}], \\ \eta &= \xi + i\zeta. \end{aligned}\right\} \tag{3.2}$$

where

This transformation leaves the ground unchanged and transforms the wing and its image on to the lines $\zeta = \pm 1$. To obtain the eigensolution, the complex potential for a uniform flow in the η plane is transformed on to the $\overline{Y}$ plane

$$\left.\begin{aligned} F(\eta) &= \phi_B + i\psi_B = U\eta, \\ U &= \text{constant}. \end{aligned}\right\} \tag{3.3}$$

where

Eliminating η between (3.2) and (3.3) gives

$$\overline{Y} = \frac{F}{U} + \frac{1}{\pi}[1 + e^{(F/U)\pi}]. \tag{3.4}$$

Since $\psi_B = U$ on $\bar{z} = 1$, we can substitute $\overline{Y} = \bar{x} + i$ and $F = \phi_B + iU$ and obtain for the wing

$$\bar{x} = \frac{\phi_B}{U} + \frac{1}{\pi}[1 - e^{\pi\phi_B/U}]. \tag{3.5}$$

This gives an inverse relation between $\bar{x}$ and ϕ_B on the wing.

For matching it is only necessary to invert this relation for the asymptotic cases of large $\bar{x}$. As $\phi_B \to \infty$ the exponential dominates and we obtain

$$\left.\begin{aligned} \bar{x} &\sim -(1/\pi)\exp\pi\phi_B/U, \\ \phi_{Bu} &\sim (U/\pi)\ln|\pi\bar{x}|. \end{aligned}\right\} \tag{3.6}$$

Here the subscript u has been added since this represents the potential on the upper surface of the wing. For the lower surface $\phi \to -\infty$. The exponential decays giving

$$\phi_{Bl} \sim U\{\bar{x} - (1/\pi)\}. \tag{3.7}$$

These asymptotic limits must match the outer flow and the flow under the wing respectively.

The solution for ϕ_A follows a similar development except that the complex velocity is transformed, rather than the complex potential. The required boundary conditions are obtained from simple corner flow in the η plane. Take

$$W(\eta) = u - iv = \eta.$$

This is transformed to the $\overline{Y}$ plane using (3.2)

$$\overline{Y} = W + (1/\pi)[1 + e^{\pi W}]. \tag{3.8}$$

On the wing, $v = -1$, so that $W = u + i$ and $\overline{Y} = \bar{x} + i$. Substituting

$$\bar{x} = u + (1/\pi)[1 - e^{\pi u}], \tag{3.9}$$

as before, we obtain asymptotic limits and attach appropriate subscripts:

$$u_u \sim (1/\pi) \ln |\pi \bar{x}|, \tag{3.10}$$

$$u_l \sim \bar{x} - (1/\pi). \tag{3.11}$$

The corresponding asymptotic values of the potential are as follows:

$$\phi_{Au} \sim (\bar{x}/\pi) \ln (\pi \bar{x}) - (\bar{x}/\pi), \tag{3.12}$$

$$\phi_{Al} \sim \tfrac{1}{2}\bar{x}^2 - (\bar{x}/\pi). \tag{3.13}$$

4. The two-dimensional wing in ground effect

This problem is particularly amenable to solution since the channel flow is one dimensional. For a flat plate airfoil (2.19) becomes

$$d^2\phi_1^c/dx^2 = 1.$$

This equation plus the boundary conditions (2.22) allow us to write the first-order solution directly

$$\phi_1^c = \tfrac{1}{2}x^2 - x.$$

The pressure distribution obtained from this solution is linear as shown in figure 6. It is worthwhile to note that to this order (i.e. α/ϵ) the perturbation velocity at the trailing edge is zero and hence free-stream conditions are obtained there. This observation alone is sufficient to yield a first approximation for the mass flow under the wing which gives the velocity everywhere in the channel from simple one-dimensional mass continuity. Referring now to figure 3, this flow model corresponds to a solution in which the rear stagnation streamline proceeds horizontally straight back from the trailing edge. It is obvious, however, that the downward momentum of the outer flow will actually cause this streamline to asymptote to a horizontal line somewhat below the height of the trailing edge, as shown, so that the mass flow in the channel must actually be somewhat less than this simple first approximation. In order to determine how much less, one must examine the outer flow.

The perturbation potential ϕ^o introduced in (2.9) must have unit downwash on the wing and, in addition, must satisfy global mass conservation. The downwash condition is satisfied by a linear distribution of sinks; to satisfy mass conservation one can add concentrated sources at the leading and trailing edges with a total mass flow equal to the mass intake of the sinks. Such concentrated sources in the outer flow correspond to the eigensolution ϕ_B in the inner flow, whereas the edge of the linear distribution corresponds to ϕ_A. Because of the fact that ϕ_B exhibits an infinite velocity at $\overline{Y} = i$, the Kutta condition serves to rule out the possibility of an eigensolution at the trailing edge, so that in the

outer flow no concentrated source is allowed there, and the leading edge must have a single source of strength two. The complex potential for this flow can be written directly as

$$F(Y) = -\frac{1}{\pi}\int_0^1 \ln(Y - Y_1)\,dY_1 + \frac{1}{\pi}\ln Y. \tag{4.1}$$

The perturbation potential evaluated on the upper surface of the wing, $z = 0$, is then

$$\phi^o = \frac{1}{\pi}\left[(x-1)\ln\left(\frac{1-x}{x}\right)+1\right]. \tag{4.2}$$

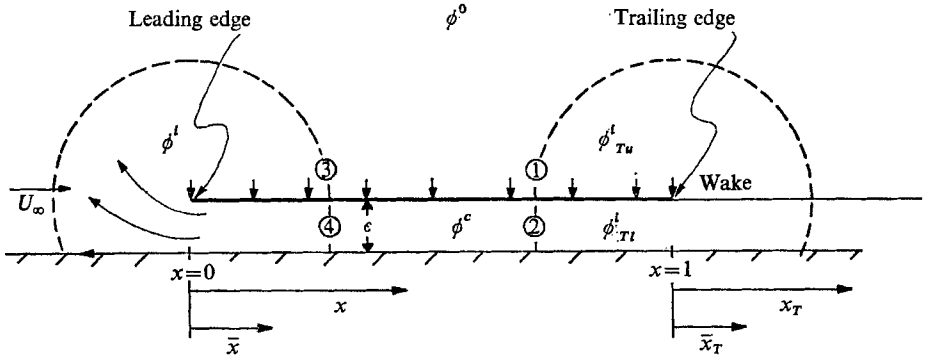

FIGURE 5. Order of matching for the two-dimensional wing in ground effect.

In order to obtain a solution valid to $O(\alpha)$ in the channel flow, it is necessary to solve for three terms of the series (2.8)

$$\phi^c = \frac{1}{\epsilon}\phi_1^c + f_1(\epsilon)\,\phi_2^c + \phi_3^c. \tag{4.3}$$

The equations (2.19) governing the higher order terms become

$$\frac{d^2\phi_2^c}{dx^2} = \frac{d^2\phi_3^c}{dx^2} = 0. \tag{4.4}$$

These equations assure that the only change in the channel flow is a small difference in the total mass flux under the wing. The pressure distribution remains linear although displaced somewhat, as shown in figure 6.

At this stage one can formulate a strategy for matching the various regions of the flow. This will be done in the following four steps as shown in figure 5:

(i) Apply the Kutta condition at the trailing edge and match the edge solution to the outer flow.

(ii) Match the channel flow to the trailing edge region. The velocity here must match to the velocity above the trailing edge, which gives a boundary condition for $d\phi^c/dx$ at the trailing edge. There is an unknown discontinuity in the potential, however, due to the circulation.

(iii) Match the outer flow to the edge flow above the leading edge.

(iv) Match the edge flow to the channel flow below the leading edge.

This gives the boundary condition for ϕ^c at the leading edge.

In actual fact this sequence for the matching is not unique. The mathematical solution of the problem simply requires expanding of all the solutions in each region and matching in the four overlap regions shown in figure 5. This order was chosen, however, because it lends some insight into how the outer flow influences the edge flow solution above the wing, and the edge flow thus provides a boundary condition for ϕ^e under the wing. These boundary conditions affect ϕ_2^e and ϕ_3^e, but not ϕ_1^e. The outer solution itself is driven by ϕ_1^e, which may be considered the cause of the leading edge source. Conceptually, it is much easier to think of the matching process as ensuring that the velocity is continuous everywhere (except right at the leading edge), although it turns out that the potential is more convenient mathematically.

Step (i). The Kutta condition at the trailing edge is imposed by stating that no eigensolution exists, since this solution gives infinite velocity at the edge. The solution is $\epsilon\phi_A$, satisfying the downwash boundary condition, plus a uniform stream and a constant. The trailing edge variable $\bar{x}_T$ is used as in figure 5.

$$\phi^i_{Tu} = (1/\pi)\,[c_1(\epsilon)\,\epsilon\bar{x}_T + c_2(\epsilon)] + \epsilon\phi_A, \tag{4.5}$$

where the factors $1/\pi$ and ϵ are written for convenience.

This is written in outer variables and expanded to $O(1)$ for the upper surface of the wing using (3.12)

$$\phi^{io}_{Tu} = \frac{1}{\pi}\left[x_T\left(\ln x_T + \ln\frac{\pi}{\epsilon} + c_1 - 1\right) + c_2\right]. \tag{4.6}$$

ϕ^{io}_{Tu} is the outer limit of the inner solution near the trailing edge on the upper surface of the wing. The outer solution in the inner variable $\bar{x}_T$ is obtained from (4.2) with $x = 1 + \epsilon\bar{x}_T$,

$$\phi^o_{Tu} = \frac{1}{\pi}\left[\epsilon\bar{x}_T \ln\left|\frac{\epsilon\bar{x}_T}{1+\bar{x}_T}\right| + 1\right]. \tag{4.7}$$

Expanded to $O(\epsilon)$ and re-expressed in outer variables, this is

$$\phi^{oi}_{Tu} = \frac{1}{\pi}\,[x_T \ln|x_T| + 1]. \tag{4.8}$$

Using the limit matching principle, ϕ^{oi} must equal ϕ^{io} which gives

$$c_1 = 1 - \ln(\pi/\epsilon); \quad c_2 = 1. \tag{4.9}$$

Selection of the constants in this manner establishes a smooth joining of the potential from the outer flow to the trailing edge region. It is now possible to determine just what influence the edge flow will have on the channel flow.

Step (ii). Beneath the trailing edge the potential is also given by (4.5) with the addition of the potential jump across the wake due to the circulation Γ.

$$\phi^i_{Tl} = \frac{1}{\pi}\left[\left(1 - \ln\frac{\pi}{\epsilon}\right)\epsilon\bar{x}_T + 1\right] - \Gamma + \epsilon\phi_A. \tag{4.10}$$

This is expressed in the channel (or outer) variable x and expanded to $O(1)$ for the region below the wing using (3.13). The resulting expression ϕ^{ic}_{Tl} is interpreted as the limit of the inner trailing edge solution as it tends toward channel flow.

$$\phi^{ic}_{Tl} = \frac{x_T^2}{2\epsilon} + \frac{1}{\pi}\left[-x_T \ln\frac{\pi}{\epsilon} + 1\right] - \Gamma. \tag{4.11}$$

This limit must equal the channel flow limit at the trailing edge. Since the value of the channel flow velocity rather than the potential is fixed by the Kutta condition, (4.11) gives the boundary condition at $x = 1$,

$$\frac{d\phi^c}{dx} = -\frac{1}{\pi}\ln\frac{\pi}{\epsilon}.$$

Also
$$f_1(\epsilon) = \ln(1/\epsilon). \tag{4.12}$$

The boundary conditions for the individual terms become

$$\left.\begin{aligned} d\phi_1^c/dx &= 0, \\ d\phi_2^c/dx &= -(1/\pi), \\ d\phi_3^c/dx &= -(1/\pi)\ln\pi. \end{aligned}\right\} \tag{4.13}$$

Step (iii). The matching over the leading edge is similar to step (i), except that the eigensolution is now allowed and all solutions are written in the leading edge variables. The solutions for the edge region are obtained from (3.5) and (3.9) (with appropriate sign changes, since the picture in figure 4 must be reversed).

The potential in the inner leading edge region is, using (3.1)

$$\phi^i = \phi_B + (1/\pi)[c_3(\epsilon)\epsilon\bar{x} + c_4(\epsilon)] + \epsilon\phi_A. \tag{4.14}$$

The matching to the outer solution in the region above the leading edge proceeds by expressing ϕ^i in the outer variable x and expanding to $O(1)$ above the edge.

$$\phi^{io} \sim \frac{1}{\pi}\left[U(\epsilon)\ln\frac{\pi x}{\epsilon} + c_3 x + c_4 - \left(x\ln\frac{\pi x}{\epsilon} - x\right)\right]. \tag{4.15}$$

It is useful to write $U(\epsilon) = U_0 + \epsilon U_1$. When this is done and the resulting expression rearranged we obtain to $O(1)$

$$\phi^{io} \sim \frac{1}{\pi}\left[U_0\ln x - x\ln x + x\left(1 - \ln\frac{\pi}{\epsilon} + c_3\right) + U_0\ln\frac{\pi}{\epsilon} + c_4\right]. \tag{4.16}$$

The inner limit of the outer solution can be obtained from (4.2).

$$\phi^{oi} = \frac{1}{\pi}[\ln x - x\ln x + x + 1]. \tag{4.17}$$

Comparison between (4.16) and (4.17) gives

$$\begin{aligned} U_0 &= 1, \\ c_3 &= \ln\pi/\epsilon, \\ c_4 &= 1 - \ln\pi/\epsilon. \end{aligned}$$

Step (iv). For the final step in the matching, the inner flow near the leading edge is expanded into the region under the wing, giving a second boundary condition to determine ϕ^c and hence Γ.

The expression for ϕ^i given by (4.14) is now expanded in outer or channel variables below the wing using the asymptotic forms for ϕ_A and ϕ_B valid beneath the wing given by (3.7) and (3.13). To $O(1)$

$$\phi^{ic} = \frac{x^2}{2\epsilon} - \frac{x}{\epsilon} - xU_1 + \frac{x}{\pi}\left(1 + \ln\frac{\pi}{\epsilon}\right) - \frac{1}{\pi}\ln\frac{\pi}{\epsilon}. \tag{4.18}$$

Applying the limit matching principle to (4.18) gives a boundary condition for ϕ^c at the leading edge

$$\phi^c(0) = -\frac{1}{\pi}\ln\frac{\pi}{\epsilon}. \tag{4.19}$$

As in (4.13), the boundary conditions for the individual terms are

$$\left.\begin{aligned}\phi_1^c(0) &= 0,\\ \phi_2^c(0) &= -(1/\pi),\\ \phi_3^c(0) &= -(1/\pi)\ln\pi.\end{aligned}\right\} \tag{4.20}$$

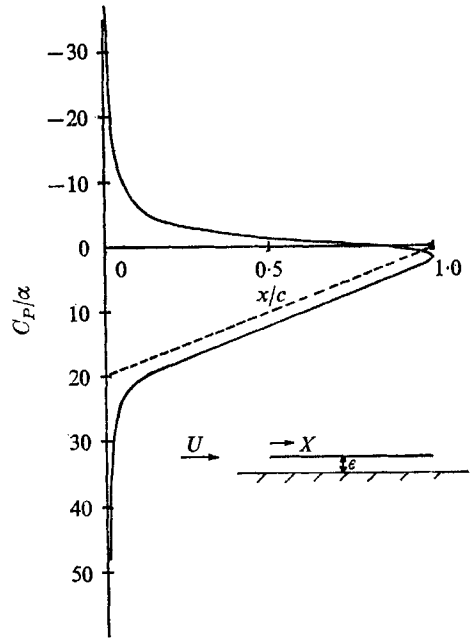

FIGURE 6. Upper and lower surface pressure distributions on a flat plate in ground effect, $\epsilon = 0{\cdot}1$. ——, numerical solution and third-order composite solution indistinguishable; – – – –, first-order solution.

The boundary condition of (4.12) and (4.19) determines the final expression for ϕ^c,

$$\phi^c = \frac{x^2}{2\epsilon} - \frac{x}{\epsilon} - \frac{x}{\pi}\ln\frac{\pi}{\epsilon} - \frac{1}{\pi}\ln\frac{\pi}{\epsilon}. \tag{4.21}$$

By comparing (4.21), (4.11) and (4.18) we obtain

$$U_1 = \frac{1}{\pi}\left[2\ln\frac{\pi}{\epsilon} + 1\right]$$

and

$$\Gamma = \frac{1}{2\epsilon} + \frac{1}{\pi}\left[2\ln\frac{\pi}{\epsilon} + 1\right]. \tag{4.22}$$

Remembering that Γ as written here is the circulation normalized by α, the lift coefficient is

$$C_L = 2\Gamma\alpha = \frac{\alpha}{\epsilon} + \frac{2\alpha}{\pi}\left(2\ln\frac{\pi}{\epsilon} + 1\right). \tag{4.23}$$

A uniformly valid composite solution for the flow above the wing can be constructed as follows:

$$\phi = (\phi^i_{Tu} - \phi^{io}_T) + (\phi^i - \phi^{io}) + \phi^o.$$

A similar formula holds below the wing with ϕ^c substituted for ϕ^o and ϕ^i_{Tl} substituted for ϕ^i_{Tu}, etc.

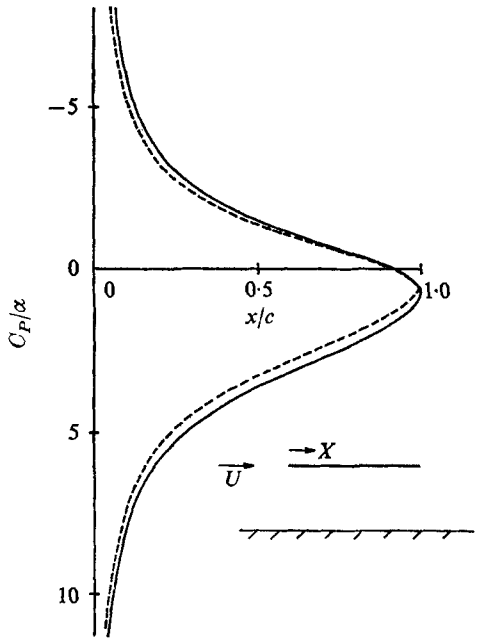

FIGURE 7. Upper and lower surface pressure distributions on a flat plate in ground effect, $\epsilon = 0{\cdot}5$. ——, numerical solution; – – –, composite solution.

The upper and lower surface pressure distributions predicted from these composite solutions were compared with a numerical linearized thin aerofoil solution which used a Glauert series with six terms and nineteen downwash control points. Boundary conditions were satisfied in the least-squares sense and the ground was represented using the method of images. Figure 6 shows the comparison for a height to chord ratio $\epsilon = 0{\cdot}1$; the agreement is essentially perfect. The pressure under the wing is linear over most of the chord with the edge flow solutions providing the proper local behaviour at the leading and trailing edges. Figure 7 shows the comparison for $\epsilon = 0{\cdot}5$. The agreement is remarkably good for this latter clearance, considering that the 'inner edge' regions for this case are so large that they essentially overlap. The outer flow gives a significant contribution to the lift.

The lift coefficient to $O(1)$ given by (4.23) is shown in figure 8 in comparison with the numerical results. It is necessary to plot $C_L\epsilon/\alpha$ *versus* ϵ in order to clearly indicate the behaviour at $\epsilon = 0$. Strangely enough, figure 8 does not reflect the same accuracy as the pressure coefficient results. This is surprising as,

presumably, (4.23) simply represents an analytic integration of pressure distribution. The resolution of this anomaly is obtained by proceeding to the next higher order, i.e. $O(\epsilon \ln \epsilon)$. It is found that a source and a doublet must be added to the leading edge in the outer flow, and a sink to the trailing edge:

$$\phi^o = \frac{1}{\pi}\left[(x-1)\ln\left(\frac{1-x}{x}\right)+1\right]+\frac{\epsilon}{\pi^2}\ln\frac{\pi}{\epsilon}\left[\ln x-\ln(1-x)+\frac{1}{x}\right]. \tag{4.24}$$

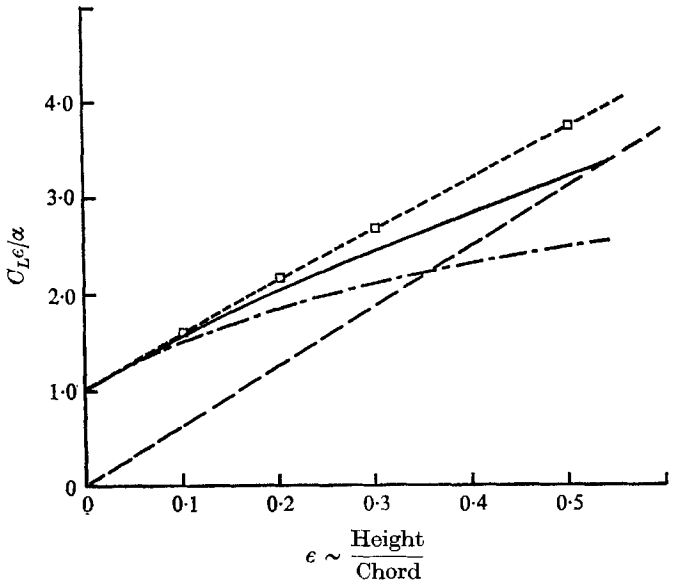

FIGURE 8. Lift coefficient for a two-dimensional flat plate airfoil in ground effect. --□--, numerical solution; —·—, solution to $O(1)$; ——, solution to $O(\epsilon \ln \epsilon)$; – – –, free stream limit $C_L\epsilon/\alpha \to 2\pi\epsilon$.

It is not worth while to go into the details of the matching which follow the previous analysis fairly closely. A small increment to the circulation is obtained.

$$\Gamma = \frac{1}{2\epsilon}+\frac{1}{\pi}\left(2\ln\frac{\pi}{\epsilon}+1\right)+\frac{\epsilon}{\pi^2}\left(4\ln\frac{\pi}{\epsilon}+2\ln^2\frac{\pi}{\epsilon}\right). \tag{4.25}$$

The important point is that nearly all of the difference between (4.23) and (4.25) arises from constants which are added to ϕ^c as the solution is carried out to $O(\epsilon \ln \epsilon)$ and $O(\epsilon \ln^2 \epsilon)$. The velocity and pressure under the wing are unaffected to this next order. These constants represent additional contributions to the total lift from the leading edge region. The addition of these higher order constants to ϕ^c considerably improves the agreement with the numerical solution, as shown in figure 8.

The above analysis provides a base for the examination of the three-dimensional lifting surface problem. It has revealed the nature of the flow beneath the wing, the nature of the edge flow regions, and the influence of the outer flow. Comparison with the numerical solution indicates the accuracy of the predicted pressure distribution and total lift.

5. Three-dimensional flat wing ground effect

We now consider the case of a flat plate wing with a straight trailing edge close to the ground.

To lowest order, the expressions for the velocity potential above and below the wing are

$$\Phi^o = x + \alpha\phi_1^o + \ldots \quad \text{and} \quad \Phi^c = x + \frac{\alpha}{\epsilon}\phi_1^c + \ldots. \tag{5.1}$$

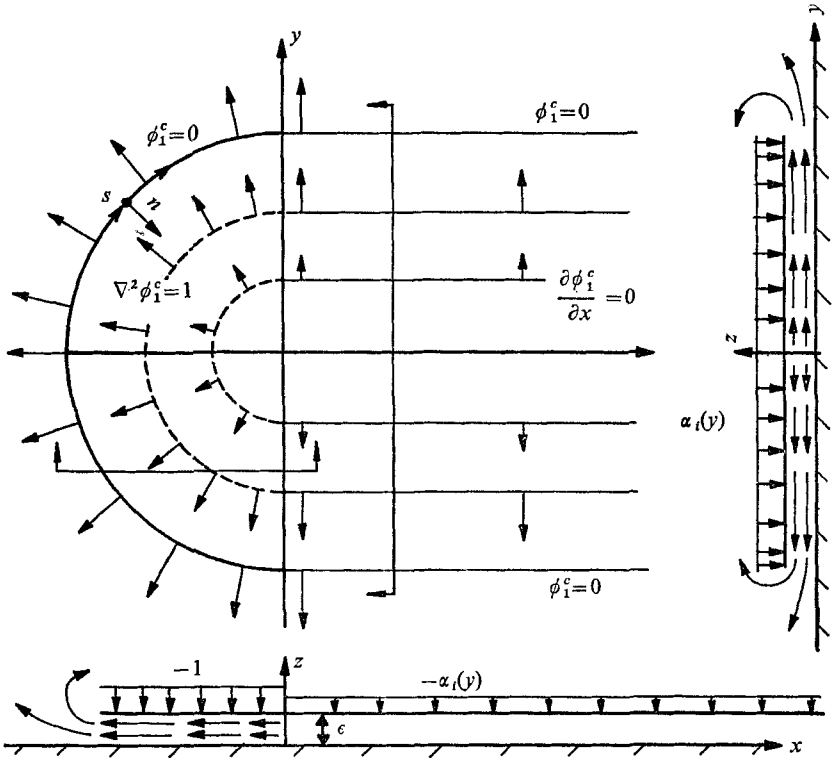

FIGURE 9. Flow perturbations beneath a flat elliptical wing with a straight trailing edge described by $\phi_1^c(x, y)$.

ϕ_1^c, which determines the essential features of the flow, is unaffected by the outer flow. For a flat wing, the function describing the shape of the lower surface is

$$\bar{g}_l(x, y) = -x. \tag{5.2}$$

Equation (2.19) becomes $$\nabla_{2D}^2\phi_1^c(x, y) = 1 \tag{5.3}$$

for the flow under the wing, with boundary conditions given by (2.22). This problem is sketched in figure 9. The flow tangency condition adds a net mass flow to the region under the wing. Because of the Kutta condition this flow cannot escape at the trailing edge but must go forward and escape via the leading and side edges. Thus the velocity under the wing is lower than free stream and lift is produced.

The solution to (5.3) is

$$\phi_1^c = \tfrac{1}{4}(x^2+y^2) + \phi_{2D}(x,y) + C, \tag{5.4}$$

where ϕ_{2D} is any two-dimensional potential flow function and C is a constant. It is simplest to take an inverse approach, choosing a potential ϕ_1^c and solving for the wing plan-form by applying the boundary condition (2.22) along the leading and trailing edges. The form of the particular solution and the trailing edge boundary condition suggest the function

$$\phi_{2D} = A[x^2 - y^2], \tag{5.5}$$

the potential function for corner flow. This assures that (5.4) satisfies the Kutta condition $\partial\phi_1^c/\partial x = 0$ at $x = 0$ so that the trailing edge lies along the y axis. The equation for ϕ_1^c can be manipulated into the form

$$\phi_1^c = [A + \tfrac{1}{4}]\left[x^2 + \frac{y^2[\frac{1}{4} - A]}{\frac{1}{4} + A} - 1\right], \tag{5.6}$$

where C has been chosen to satisfy the leading edge boundary condition at $x = -1$, $y = 0$. $A = \frac{1}{4}$ corresponds to an infinite aspect ratio wing in ground effect, $A = -\frac{1}{4}$ corresponds to a wing of zero ratio, although the theory is not valid for $AR \sim O(\epsilon)$; AR is the aspect ratio $(2b)^2$/area, where b is the semispan/chord ratio.

Applying the condition $\phi_1^c = 0$ gives the equation for the leading edge

$$x_{LE}^2 + (y_{LE}/b)^2 = 1, \tag{5.7}$$

which is the equation of an ellipse with

$$b = [(\tfrac{1}{4} + A)/(\tfrac{1}{4} - A)]^{\frac{1}{2}}.$$

After solving for A, the potential ϕ_1^c for a flat elliptical wing becomes

$$\phi_1^c = \frac{b^2}{2(b^2+1)}\left[x^2 + \left(\frac{y}{b}\right)^2 - 1\right]. \tag{5.8}$$

In the wake $\phi_1^c(y)$ has the value

$$\phi_1^c = \frac{b^2}{2(b^2+1)}\left[\left(\frac{y}{b}\right)^2 - 1\right]. \tag{5.9}$$

The spanwise distribution of circulation to this order is $\Gamma(y) = -(\alpha/\epsilon)\,\phi_1^c(y)$.

$$\Gamma(y) = \left(\frac{\alpha}{\epsilon}\right)\frac{1}{2}\frac{b^2}{b^2+1}\left[1 - \left(\frac{y}{b}\right)^2\right] \tag{5.10}$$

since the outer flow perturbations are $O(\alpha)$. Thus, the variation of lift along the span is parabolic.

The lift coefficient, lift/$\frac{1}{2}\rho U_\infty^2$ area where U_∞ is the free-stream velocity, of this wing is

$$C_L = \left(\frac{\alpha}{\epsilon}\right)\frac{8}{3\pi}\frac{b^2}{b^2+1}. \tag{5.11}$$

The semi-circular wing, $b = 1$, has half the lift coefficient of the infinite wing. The results for $b/c \to \infty$ do not approach the two-dimensional results since the

wing remains elliptic in this limit. Although the flow becomes locally two dimensional, since the outboard chords are shorter in comparison to their height above the ground, the lift decreases in proportion to the square of the local chord in contrast to the infinite fluid case. For a two-dimensional wing to lowest order

$$C_{L_{2D}} = (\alpha/\epsilon), \tag{5.12}$$

whereas for $b/c \to \infty$

$$C_L = \frac{\alpha}{\epsilon}\frac{8}{3\pi}. \tag{5.13}$$

To this order, all of the lift comes from the increased pressures on the bottom of the wing. As in the two-dimensional case, the distribution of lift is linear along the chord to lowest order, although at a reduced magnitude due to the finite span. The spanwise lift distribution produced by the elliptical wing is parabolic because a lift distribution which is linear with the same slope along every chord produces a local lift proportional to the local chord squared. Since

$$c(y) \sim \sqrt{[1-(y/b)^2]}$$

the lift distribution

$$L(y) \sim 1-(y/b)^2.$$

Figure 9 shows the flow perturbations associated with this solution for a flat elliptical wing. The downwash boundary condition on $z = \epsilon$ induces a horizontal flow in the region below the wing. In the three-dimensional case, there is the additional feature of a trailing vortex wake. For this wing, the induced downwash $\alpha_i(y)$ as given by (2.20) is constant in the wake and of magnitude

$$\alpha_i = 1/(b^2+1). \tag{5.14}$$

For b approaching infinity, $\alpha_i(y)$ goes to zero which is the proper limit for infinite aspect ratio; for b approaching zero, α_i goes to one, the slender body limit.

Since the induced downwash in the wake is constant, this wing has minimum drag for a given lift. An exact solution to the Trefftz plane flow of a wing in ground effect has been found by Haller (1936), who also obtained the result that the optimum lift distribution becomes parabolic as the clearance goes to zero. It is a curious result that the elliptic plan-form is optimal for a wing in ground effect for all aspect ratios. The problem of minimizing induced drag for a variety of vehicle guideway configurations with small clearances has been discussed by Barrows & Widnall (1970).

The matching procedure applied to the two-dimensional problem can also be applied locally to the edges of the three-dimensional wing. The perturbation velocities of $\phi_1^c(x,y)$ are normal to the leading and side edges and the two-dimensional edge flow solution can be applied to lowest order since the radius of curvature is of $O(1)$, which is large in comparison to the width of the edge flow region, of $O(\epsilon)$. The details will not be carried out here; the results will be stated with reference to the two-dimensional results. The outer flow potential ϕ^o can be constructed from a known distribution of sources and sinks located over the wing and wake. Matching the channel perturbation potential to this outer flow through local normal edge flows gives a boundary condition on $\partial\phi^c/\partial x$ at the trailing edge and ϕ^c at the leading edge.

At a point s on the leading edge the inner limit of the outer solution will be

$$\phi^{oi} \sim \frac{U(s)}{\pi} \ln n - \frac{1}{\pi}[n \ln n - A(s)], \tag{5.15}$$

where n is a local normal co-ordinate. $U(s)$ is the local normal velocity, $\partial\phi_1^c/\partial n$. $A(s)$ is the $O(1)$ effect due to distant sources. Matching this expression through a local edge flow solution gives the boundary conditions for ϕ^c at the leading edge.

$$\phi^c(s) = -\frac{U(s)}{\pi} \ln \frac{\pi}{\epsilon} - \frac{U(s)}{\pi} + \frac{A(s)}{\pi}. \tag{5.16}$$

Similarly, for a trailing edge in three-dimensional flow, the outer flow solution will behave locally as

$$\phi_T^{oi} = \frac{1-\alpha_i}{\pi}[x_T \ln x_T] + B(y) + C(y)x_T. \tag{5.17}$$

The first term comes from the discontinuity in sink strength at the trailing edge where the downwash changes from α to α_i as indicated in figure 9. $B(y)$ and $C(y)$ are $O(1)$ effects from distant sources. Matching this through a local trailing edge solution gives a boundary condition for $\partial\phi^c/\partial x$ at the trailing edge to $O(1)$.

$$\frac{\partial\phi^c}{\partial x}(0) = -\frac{1-\alpha_i}{\pi} \ln \frac{\pi}{\epsilon} + C(y). \tag{5.18}$$

Restating the governing equations for the individual terms in the expansion of (2.7) for ϕ^c, the potential beneath the wing, we have

$$\nabla^2\phi_1^c = 1, \tag{2.18}$$

$$\nabla^2\phi_2^c = 0, \quad \nabla^2\phi_3^c = 0. \tag{2.19}$$

The matching has provided the boundary conditions for these equations to be applied at the leading and trailing edges. At a leading edge

$$\left.\begin{aligned} \phi_1^c &= 0, \\ \phi_2^c &= -\frac{1}{\pi}\frac{\partial\phi_1^c}{\partial n}, \\ \phi_3^c &= -\frac{1}{\pi}[1+\ln\pi]\frac{\partial\phi_1^c}{\partial n} + \frac{A(s)}{\pi}. \end{aligned}\right\} \tag{5.19}$$

At a trailing edge

$$\left.\begin{aligned} \frac{\partial\phi_1^c}{\partial x} &= 0, \\ \frac{\partial\phi_2^c}{\partial x} &= -[1-\alpha_i]\frac{1}{\pi}, \\ \frac{\partial\phi_3}{\partial x} &= -[1-\alpha_i]\frac{\ln\pi}{\pi} + C(y). \end{aligned}\right\} \tag{5.20}$$

With these equations, the lifting surface problem for a wing in close proximity to the ground becomes a direct although perhaps tedious problem.

It is of interest to carry the semicircular wing to next order. This can be done

relatively simply because $\partial\phi_1^c/\partial n$ is constant around the leading edge for this particular case. Stating the problem for $\phi_2^c(x,y)$, we have

$$\left.\begin{aligned} \nabla^2\phi_2^c(x,y) &= 0, \\ \phi_2^c &= -\frac{1}{2\pi} \quad \text{at the leading edge,} \\ \frac{\partial\phi_2^c}{\partial x} &= -\frac{1}{2\pi} \quad \text{at the trailing edge.} \end{aligned}\right\} \tag{5.21}$$

The solution can be found using complex variable image techniques.

Using $z = y - ix$ for convenience

$$\phi_2^c + i\psi_2^c = \frac{1}{2\pi^2}\left[-(z-1)\ln(z-1) + \left(\frac{1}{z}-1\right)\ln\left(\frac{1}{z}-1\right)\right.$$
$$\left. + (z+1)\ln(z+1) - \left(\frac{1}{z}+1\right)\ln\left(\frac{1}{z}+1\right) - 2\ln z\right] - \frac{1}{2\pi}. \tag{5.22}$$

The value of $\phi_2^c(y)$ along the trailing edge gives the additional circulation $\Gamma_2(y)$,

$$\Gamma_2(y) = -\alpha\ln\frac{1}{\epsilon}\phi_2^c = -\alpha\ln\frac{1}{\epsilon}\left[\frac{1}{2\pi^2}\left(\frac{1-y^2}{y}\right)\ln\frac{1-y}{1+y} - \frac{1}{2\pi}\right]. \tag{5.23}$$

The additional contribution to the lift is

$$C_{L_2} = \alpha\ln\left(\frac{1}{\epsilon}\right)\frac{4}{\pi}\left(\frac{1}{4} + \frac{1}{\pi} - \frac{1}{\pi^2}\right). \tag{5.24}$$

For a circular wing to $O(\alpha\ln\epsilon)$

$$C_L = \frac{\alpha}{\epsilon}\frac{4}{3\pi} + \alpha\ln\left(\frac{1}{\epsilon}\right)\left(\frac{4}{\pi}\right)\left(\frac{1}{4} + \frac{1}{\pi} - \frac{1}{\pi^2}\right). \tag{5.25}$$

The next term would be $O(1)$ and would involve contributions for both the upper and lower surfaces.

6. Comparison with numerical lifting surface theory

Numerical calculations for two elliptical wings with straight trailing edges in an infinite free stream and in ground effect were performed using the method discussed by Ashley, Widnall & Landahl (1965). Two wings were chosen having semispan to chord ratios of 1 and 0·5. The numerical method was developed for wings in an infinite fluid with moderate aerodynamic influence from nearby surfaces. It was felt that for this technique convergence could not be assured much below $\epsilon = 0{\cdot}05$. Of course, this region of strong influence is just where the analytic solution is expected to be valuable. The numerical results for lift coefficient are summarized in figure 14.

For the wing in ground effect, $C_L\epsilon/\alpha$ is plotted *versus* ϵ to focus on the behaviour for small clearances. The first-order linear theory predicts $C_L\epsilon/\alpha$ to be a function only of aspect ratio. The limits for $b/c = 0{\cdot}5$ and $1{\cdot}0$ are indicated at $\epsilon = 0$. For large clearances C_L approaches the free stream limit C_{L_∞} so $C_L\epsilon/\alpha$ increases

linearly with ϵ. This asymptote, $C_{L_\infty}\epsilon/\alpha$ is indicated in figure 10. The results of the numerical lifting surface calculations for the two finite wings in ground effect are shown for $\epsilon = 0{\cdot}05$, $0{\cdot}1$, $0{\cdot}3$ and $0{\cdot}5$.

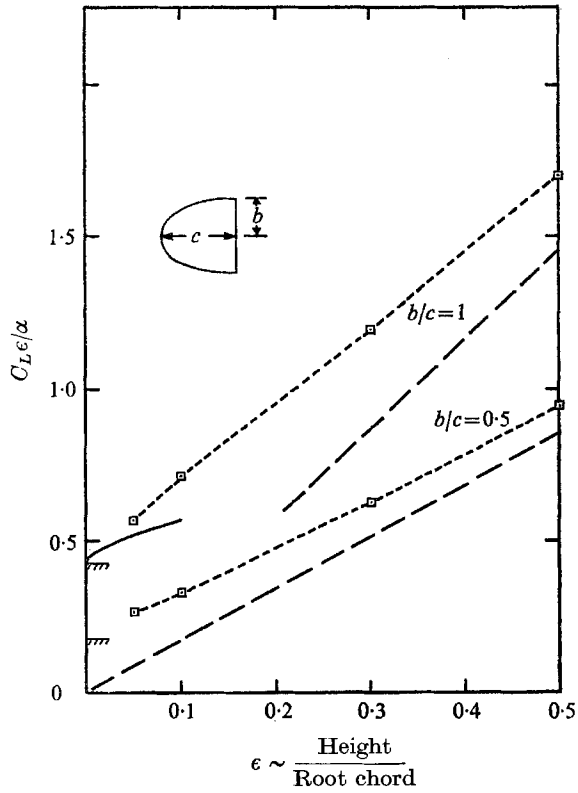

FIGURE 10. Comparison of numerical lifting surface theory with the analytic solution for a flat elliptical wing in ground effect with clearance ϵ. —⊡—, numerical solution; ////, lowest order solution; ——, two-term solution; ————, free stream limit $C_L\epsilon/\alpha \to C_{L_\infty}\epsilon/\alpha$.

The numerical results indicate a reasonable approach to the $\epsilon = 0$ limit. For finite values of ϵ, however, one is tempted to proceed to higher order in ϵ, the next terms in the expansion for $C_L\epsilon/\alpha$ being $\sim O(\epsilon \ln \epsilon)$ and $O(\epsilon)$. This proved to be quite easy for the semicircular wing and the two-dimensional wing because the perturbation mass flow normal to the edges is constant.

The two-term expansion for the semicircular wing as given by (5.25) is shown in figure 10 and shows reasonable consistency with the numerical results, although one more term in the expansion would be required for the same quality of comparison as shown for the two-dimensional results.

A comparison of the lift distribution on a semicircular wing in ground effect as predicted by the simple first-order theory and as obtained using numerical lifting surface techniques is shown in figure 11 for a height to root chord ratio $\epsilon = 0{\cdot}05$. The first-order theory gives the simple linear lift distribution. The lifting surface result contains the proper leading and trailing edge behaviour

which would appear in the analytic solution for higher orders in ϵ as in the two-dimensional case. The agreement is quite good in those regions away from the edge.

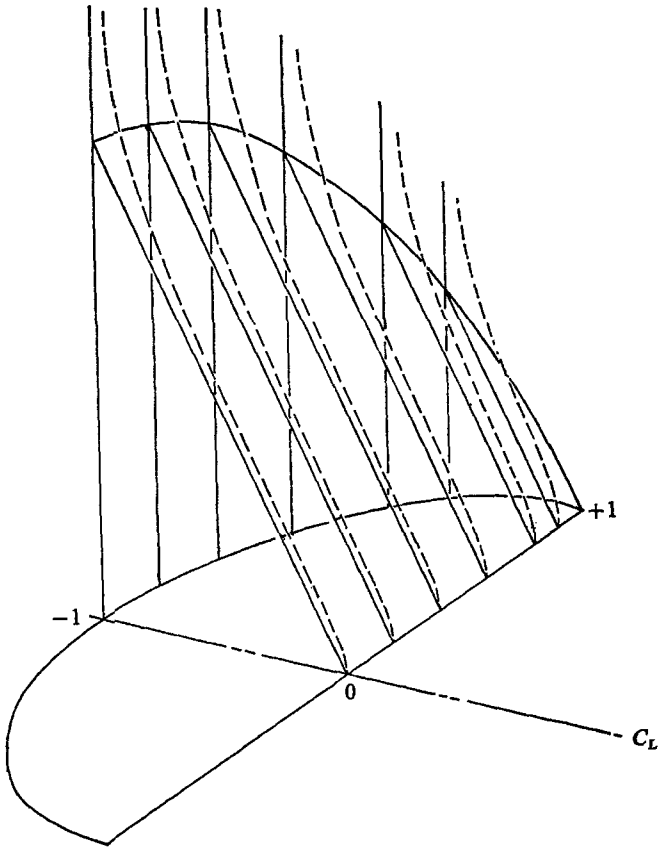

FIGURE 11. Comparison of analytic and numerical results for lift distribution on a semi-circular wing in ground effect, $\epsilon = 0{\cdot}05$. ——, first-order theory; – – – –, numerical lifting surface theory.

7. Summary and conclusions

Using the method of matched asymptotic expansions, the linearized lifting surface problem for a wing very close to the ground has been formulated. Unlike the lifting surface problem in an infinite fluid, the lifting problem close to the ground is a direct problem involving a source/sink rather than a vortex distribution. Flow in the confined region beneath the wing and wake is a two-dimensional channel flow with known boundaries and known mass addition, coming from the flow tangency boundary condition on the lower surfaces. The thickness and lifting problems do not decouple for a wing in strong ground effect, in fact, to lowest order the lift coefficient is only a function of the shape of the wing lower surface and planform.

The two-dimensional linearized flow problem for a lifting flat plate close to the ground is particularly amenable to solution by this method. Analytic solutions may be obtained up to fourth order (i.e. $\epsilon \ln \epsilon$) without undue difficulty. Higher order terms are available, although their usefulness is questionable. The third-order result for the pressure distribution on the upper and lower surfaces are remarkably accurate, showing good agreement with numerical calculations for clearances as large as $\epsilon = 0{\cdot}5$. The singularity at the leading edge shown by the flat plate solution could be removed by a method similar to Lighthill's technique for correcting flows around blunt leading edges.

A remarkably simple analytic solution is obtained in the case of an optimally loaded flat elliptical wing with a straight trailing edge. The lift distribution for minimum induced drag is a distribution which is linear along the chord, dropping to zero at the trailing edge to satisfy, to lowest order, the Kutta condition. An analytic expression (5.13) gives the lift coefficient of such a wing to $O(1/\epsilon)$; this equation is valid for all aspect ratios greater than ϵ.

For the semi-circular flat wing the flow perturbations can be found analytically to $O(\ln \epsilon)$ giving a two-term expansion for C_L. The analytical results are compared with numerical results from lifting surface theory for a finite wing in ground effect. For good accuracy up to $\epsilon = 0{\cdot}1$, the solution should be carried to $O(\alpha)$. In the expected range of operation of high speed ground transportation vehicles, say $\epsilon = 0{\cdot}01$, the simple first-order solution should give accurate results.

REFERENCES

Ashley, H. & Landahl, M. 1965 *Aerodynamics of Wings and Bodies.* Reading, Mass.: Addison Wesley.

Ashley, H., Widnall, S. & Landahl, M. 1965 New directions in lifting surface theory. *AIAA J.* **3**, 3.

Bagley, J. A. 1960 Pressure distribution on two-dimensional wings near the ground. *RAE Rep. Aero.* 2625.

Barrows, T. M. & Widnall, S. E. 1970 Optimum lift-drag ratio for a ram wing tube vehicle. To appear in *AIAA J.*

Haller, P. de 1936 La portance et la trainée induite minimum d'une aile au voisinage du sol. *Mitt. Inst. Aerodyn. Zurich,* **5**, 99.

Kaario, T. J. 1935 Process for eliminating friction between a surface vehicle and the surface. *Finnish Patent,* no. 18630.

Pistolesi, E. 1937 Ground effect—theory and practice. *NACA TM* no. 828.

Strand, T., Royce, W. W. & Fujita, T. 1962 Cruise performance of channel-flow ground effect machines. *J. Aero. Sci.* **29**, 702.

Tomotika, S., Hasimoto, Z. & Urano, K. 1951 The forces acting on an aerofoil of approximate Joukowski type in a stream bounded by a plane wall. *Quart. J. Mech. Appl. Math.* **4**, 289.

Van Dyke, M. 1964 *Perturbation Methods in Fluid Mechanics.* New York: Academic.